Clim Dyn (2007) 29:791–805
DOI 10.1007/s00382-007-0257-6

# A European pattern climatology 1766–2000

**Carlo Casty · Christoph C. Raible · Thomas F. Stocker · Heinz Wanner · Jürg Luterbacher**

Received: 28 December 2005 / Accepted: 21 March 2007 / Published online: 22 May 2007


**Abstract** Using monthly independently reconstructed gridded European fields for the 500 hPa geopotential height, temperature, and precipitation covering the last 235 years we investigate the temporal and spatial evolution of these key climate variables and assess the leading combined patterns of climate variability. Seasonal European temperatures show a positive trend mainly over the last 40 years with absolute highest values since 1766. Precipitation indicates no clear trend. Spatial correlation technique reveals that winter, spring, and autumn covariability between European temperature and precipitation is mainly influenced by advective processes, whereas during summer convection plays the dominant role. Empirical Orthogonal Function analysis is applied to the combined fields of pressure, temperature, and precipitation. The dominant patterns of climate variability for winter, spring, and autumn resemble the North Atlantic Oscillation and show a distinct positive trend during the past 40 years for winter and spring. A positive trend is also detected for summer pattern 2, which reflects an increased influence of the Azores High towards central Europe and the Mediterranean coinciding with warm and dry conditions. The question to which extent these recent trends in European climate patterns can be explained by internal variability or are a result of radiative forcing is answered using cross wavelets on an annual basis. Natural radiative forcing (solar and volcanic) has no imprint on annual European climate patterns. Connections to $CO_2$ forcing are only detected at the margins of the wavelets where edge effects are apparent and hence one has to be cautious in a further interpretation.

**Keywords** Independent climate field reconstructions · Europe · Climate patterns · Combined EOFs

## 1 Introduction

It is well known that mean monthly geopotential height fields for the mid-troposphere determine monthly European surface precipitation and temperature fields (Namias 1948; Hurrell 1995; Hurrell and van Loon 1997; Xoplaki et al. 2003, 2004; Casty et al. 2005a). These atmospheric processes are connected with quasi-stationary patterns of climate variability like the North Atlantic Oscillation (NAO), which generates typical temperature and precipitation patterns of the whole Atlantic and European sector (e.g., Hurrell 1995; Hurrell and van Loon 1997; Wanner et al. 2001; Hurrell 2003). However, they explain only parts of the climate variability over a defined region because they are also affected by spatial and temporal non-stationary behaviour (Casty et al. 2005a; Raible et al. 2006). Stephenson et al. (2003) define a climate pattern simply as a spatial pattern that is derived using a particular statistical method. A prominent example is the use of Empirical Orthogonal Functions (EOF, e.g., Barnston and

**Electronic supplementary material** The online version of this article (doi:10.1007/s00382-007-0257-6) contains supplementary material, which is available to authorized users.

C. Casty (✉) · C. C. Raible · T. F. Stocker
Climate and Environmental Physics, Physics Institute, University of Bern, Bern, Switzerland
e-mail: casty@climate.unibe.ch

H. Wanner · J. Luterbacher
Climatology and Meteorology, Institute of Geography, University of Bern, Bern, Switzerland

C. C. Raible · T. F. Stocker · H. Wanner · J. Luterbacher
NCCR Climate, University of Bern, Bern, Switzerland

Lizevey 1987). However, statistically derived patterns do not guarantee to be the result of an underlying physical process (Dommenget and Latif 2002; Hannachi et al. 2006). Physically meaningful patterns are defined as climate modes (Stephenson et al. 2003). For example, applying an EOF analysis to combined pressure, temperature, and precipitation fields, Fraedrich et al. (1993) present different patterns, one resembling the NAO and another one a blocking type pattern over Europe, and show the importance of transient and stationary wave activity to generate these patterns. The goal of this paper is to describe and classify the European climate variability back to 1766 on a seasonal basis using independent reconstructions for pressure, precipitation, and temperature.

Using observations, reanalysis data, proxy reconstructions, and general circulation models (GCM), a variety of dynamical hypotheses regarding the formation of the NAO low-frequency variability was proposed. Explanations range form purely internal atmospheric variability (James and James 1989), the inclusion of external radiative forcing factors (Graf et al. 1994; Raible et al. 2006; Yoshimori et al. 2005), feedbacks via stratosphere–troposphere interaction (Perlwitz and Graf 2001; Shindell et al. 2004) to ocean–atmosphere coupling involving the North Atlantic (Bjerknes 1962; Groetzner et al. 1998) or the tropical Pacific (Rowntree 1972; Fraedrich 1994; Hoerling et al. 2001). Raible et al. (2001) combined the tropical response to the NAO and the regional sea surface temperature (SST) linkage of the NAO and suggested two decadal regimes: a hemispheric regime dominated by interannual variability in the North Atlantic and a regional regime with enhanced decadal variations. The NAO trend of the last few decades until the end of the twentieth century to its positive phase is of specific interest. Some authors (Hoerling et al. 2001, 2004; Hurrell et al. 2004) suggest a linkage to the tropical Indian Ocean whereas others find that this trend is not statistically different from the climatological level of atmosphere–ocean variability (Wunsch 1999; Schneider et al. 2003; Raible et al. 2005). Recently, Latif et al. (2004) showed in a modelling study a connection between the SST and the meridional overturning circulation (MOC) implying a potential of predictability in the Atlantic–European region.

Observations in the form of gridded data sets (reanalyses; e.g., Kalnay et al. 1996; Kistler et al. 2001; Mitchell and Jones 2005) are often limited in length. Thus, there is a necessity to construct longer gridded data sets to further understand the variability and covariability of climate patterns und related climate variables. Due to its large number of long and high-quality instrumental station data, Europe is an ideal area to generate spatially and temporally high resolution climate field reconstructions (CFRs) of temperature, precipitation, and pressure covering the last centuries (e.g., Brönnimann and Luterbacher 2004; Casty et al. 2005a, b; Jones and Mann 2004; Luterbacher et al. 2002; 2004; Mann et al. 2005; Pauling et al. 2006; Rutherford et al. 2003, 2005; Xoplaki et al. 2005). To assess the covariability of climate relevant variables, these CFRs have to be independently estimated, with no overlap in the used proxy data in order to avoid circular statements during the interpretation process (Casty et al. 2005a, b). We present independently estimated CFR for land surface temperatures (LST), land surface precipitation (LSP), and the 500 hPa geopotential height field (Z500) for the European sector back to 1766. We further investigate the relationship between these variables for all seasons leading to different climate patterns of the combined LST, LSP, and Z500 fields.

Section 2 gives insights into the data and methods to compute independent LST, LSP, and Z500 CFR over Europe back to 1766. Seasonal time series for temperature and precipitation are presented in Sect. 3. Spatial correlations between seasonal European temperature and precipitation fields since 1766 are shown. Taking into account the Z500, combined EOF are calculated in order to classify and describe the first three leading patterns of variability over Europe for the last 235 years. Then, the connection of the dominant annual pattern to radiative forcing is stressed. The paper is discussed and summarised in Sect. 4.

## 2 Data and methods

Casty et al. (2005a) calculated monthly independent CFRs for European LST, LSP, and the Z500 back to 1766. The independent CFR share no common predictors (i.e., temperature is only reconstructed from temperature data, precipitation reconstructions rely solely on station precipitation; sea level pressure reconstructions are based on station pressure series only), therefore we avoid circular statements during the interpretation process when considering multiple CFRs. CFR are gridded fields, which are generated by regressing a spatial network of station data against modern gridded climate data (e.g., reanalysis). Transfer functions via Principal Component (PC) regression are calculated during periods where both information, the station data and the gridded climate information (e.g., Kalnay et al. 1996; Kistler et al. 2001; Mitchell and Jones 2005) are available. Stationary behaviour is assumed, i.e., relations between station data and reanalysis do not change over time. These transfer functions are finally fed with the long instrumental station data in order to receive a spatial evolution of the past climate. The spatial resolution of the LST and LSP CFR is $0.5° \times 0.5°$ equal to the reanalysis (CRU TS2; 1901–1995; Mitchell and Jones 2005) used for calibration of the transfer functions. The choice of the CRU data is mainly motivated by its length compared with

e.g., ERA-40 data (Simmons and Gibson 2000). The long calibration period reduces the influence of calibrating the transfer function against recent climate trends (Rutherford et al. 2003). For the Z500 reconstruction the NCEP reanalysis (Kalnay et al. 1996; Kistler et al. 2001) on a 2.5° × 2.5° grid over the 1948–1995 period is used. Note that the Z500 reconstruction completely relies on statistical transfer functions with sea level pressure (SLP) measurements. Schmutz et al. (2001), Luterbacher et al. (2002), and Brönnimann and Luterbacher (2004) showed that it is possible to statistically reconstruct high-quality upper-level pressure fields using surface pressure data. The study area is chosen from 30–80°N to 50°W–40°E, which fully captures the well-known climate patterns of variability for the European region (Wanner et al. 2001). The independent CFRs presented in this study rely fully on instrumental data. This reduces their length due to a limited number of pressure station data prior to 1766. The statistical reconstruction method is fully described in Luterbacher et al. (2002, 2004) and Casty et al. (2005a). For the spatial distribution of the station data over time the reader is referred to Casty et al. (2005a).

Figure 1a–c reveal the temporal evolution of the station data network of the three CFRs highlighted in dotted lines. Note that there are negligible differences between the temporal station data evolution for each seasons. Therefore, we only plotted the station data for winter. The changing number of station data over time has to be considered using a nested statistical model approach, i.e., for each specific combination of station data the calibration steps have to be newly performed. For the Z500 reconstructions, 176 nested statistical models were developed, 373 for the LSP and finally 422 statistical models were needed for the LST reconstruction. In Figs. 1a–c also the performance of reconstructions is quantitatively expressed by the Reduction of Error measure (RE; Lorenz 1956):

$$\mathrm{RE} = 1 - \frac{\sum_{i=i}^{n} (x_i - \hat{x}_i)^2}{\sum_{i=i}^{n} (x_i - \bar{x}_c)^2},$$

where $\bar{x}_c$ is the mean of the calibration period (1901–1960 for LST and LSP; 1948–1978 for Z500). $\hat{x}_i$ denotes the reconstructed value and $x_i$ reflects the observed value of independent data during the verification period (1961–1995 for LST and LSP; 1979–1995 for Z500). RE ranges from $-\infty$ to 1. An RE value of 1 represents a perfect reconstruction, i.e., the reconstructed value fits perfectly to the independent data throughout the calibration period. A value of 0 is achieved when the reconstructed value resembles the calibration mean. Negative values indicate no skill of the reconstructions. Except for summer, seasonal Z500 reconstructions perform well with RE values higher than 0.5 (Fig. 1a). LST (Fig. 1b) performs even better than the Z500 reconstruction with overall RE values higher than 0.6. Winter and summer show lower skill than spring and autumn. Precipitation reconstructions perform worse than Z500 and LST (Fig. 1c). Pauling et al. (2006) discuss limitations of a high-resolution precipitation reconstruction over Europe. The spatial picture of the RE shows similarities for all parameters and seasons. The skill of reconstructions is reduced at the margins of the study area due to missing station information (not shown). For the earlier part, more station data are available from central Europe leading to better seasonal reconstruction in this area.

In order to detect climate patterns and to describe their variability in space and time, we perform combined linear EOF analyses (e.g., Bretherton et al. 1992) of monthly Z500, LST, and LSP CFRs for 1766–2000. The LST and LSP are interpolated on the 2.5° grid of the Z500 CFR for a better comparison. For each LST, LSP, and Z500 fields, normalised anomalies are calculated (the 1766–2000 mean annual cycle is subtracted and then divided by the standard deviation over the full period). The three climate fields (Z500 has 777 grid points; LST and LSP have each 444 grid points over land) are then summarized into a combined climate state vector of normalised seasonal data (similar to Fraedrich et al. 1993; Casty et al. 2005a). Seasons are combined by including monthly data of the three months that belong to a climatological season (e.g., winter is December through February). This results in 705 time steps for each seasonal EOF of the last 235 years. Note that the patterns described in this paper are statistical constructs.

To compare the PCs of the combined EOF analysis with the temporal evolution of the external forcing, we use wavelet, cross wavelet, and squared wavelet coherence techniques (Torrence and Compo 1998; Jevrejeva et al. 2003; Grinsted et al. 2004). The wavelet analysis is an extension to classical Fourier transformation methods, where the wavelet transformation expands time series in the time–frequency space. Thus, it is possible to find temporally localised periodicities. With the cross wavelet spectrum and the squared wavelet coherence we examine relationships in the time frequency space between two time series. The cross wavelet spectrum focuses on the common enhanced spectral power (or variability) of both time series, whereas the squared wavelet coherence could be interpreted as a localised correlation coefficient in the time–frequency domain. The interpretation of cross wavelet spectrum and squared wavelet coherence is not straightforward. We restrict our study to discuss only significant peaks (at a level of 95%) with respect to red noise, if the power is significantly enhanced in the time–frequency domain of the cross wavelet, the wavelet coherence is significantly high, and the phase shift for the spectral band is uniform. If only one significant peak appears in either method (cross wavelet or the wavelet coherence) or the

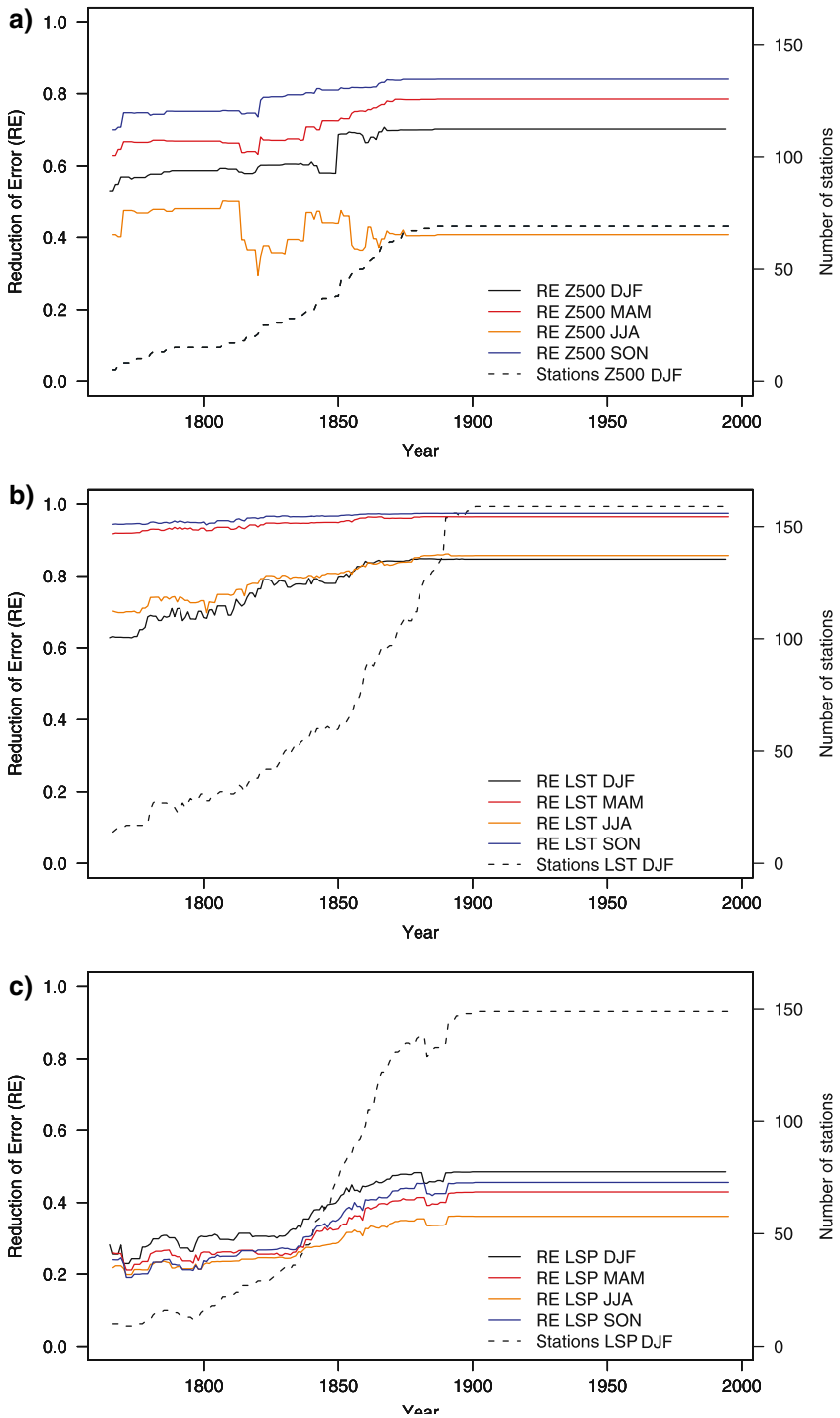


**Fig. 1** **a** Area-averaged reduction of error (*RE*) statistics for the 500 hPa geopotential height (Z500) reconstruction for each season since 1766 (*solid lines*, left *y*-axis). The temporal evolution of the station data for winter (DJF) of the Z500 reconstruction is plotted with dotted lines (right *y*-axis). The maximum number of station data is 59. **b** Same as **a**, but for land surface temperatures (*LST*). The maximum number of station data is 159. **c** Same as **a**, but for the land surface precipitation (*LSP*) reconstruction. The maximum number of station equals 149

phase shift changes in a spectral band over time, we interpret this as randomness. In our case the PCs of the combined EOF as a representation of the large-scale atmospheric behaviour and different external forcings are examined with these techniques. Three different external forcing time series are used 1766–2000: the solar forcing is based on Lean et al. (1995) and Crowley (2000), the volcanic forcing is from Crowley (2000) and the $CO_2$ data stem from Etheridge et al. (1996).

## 3 Results

### 3.1 Seasonal European temperature variations 1766–2000

European winter temperature anomalies (Fig. 2a; reference period 1901–2000) prior to 1900 are lower than during the twentieth century. The variability is high throughout the 1766–2000 period (as expressed by the standard deviation

$\sigma$ = 0.78°C) and unfiltered uncertainties (grey shading), defined as ±2 standard errors (Briffa et al. 2002), are rather small. These uncertainties are about 0.4°C in 1766 and decrease to 0.2°C for the year 1900. After 1900 a strong increase in temperature can be detected, which leads to warmest conditions ever experienced during the last 235 years. Note that temperatures from 1901 to 2000 are identical to the CRU TS2 reanalysis (Mitchell and Jones 2005).

The spring temperature curve (Fig. 2b) is similar to winter; however, conditions were as warm as the twentieth century mean from 1766 to 1820. It exhibits a cooling until 1900 and again an increase to warmer than average temperatures after 1900. The uncertainties are similar to winter, starting at 0.4°C and decrease to values of about 0.2°C for 1900. The spring temperature variability ($\sigma$ = 0.53°C) is lower than for winter.

Summer temperatures (Fig. 2c) 1766–1871 are higher than during the twentieth century. They decrease remarkably to low values for the 1872–1927 period. Following, a temperature increase is found and for the 1928–1965 period. After a slight cold phase 1966–1984, recent temperature anomalies again are positive. Summer temperature variability is low ($\sigma$ = 0.38°C) and the uncertainties are largest compared with other seasons. They range from 0.45°C in the year 1766 to 0.24°C about 1900.

Autumn temperatures (Fig. 2d) for the 1766–1800 period are similar to twentieth century conditions and decrease to persistent cold conditions until 1925. Afterwards, a strong increase in autumn temperature is detected and high levels persist from 1929 to 1954. Then, temperatures decrease to lower than average values 1967–1980. In recent times, autumn temperatures are strongly increasing. Temperature variability is higher than for summer with $\sigma$ = 0.48°C. The uncertainties of the reconstruction are again similar to winter and spring with values ranging from 0.4 to 0.2°C.

Using a similar methodological approach, Luterbacher et al. (2004) reconstructed European winter and summer temperatures back to 1500, based on a combination of early temperature, pressure station data, and proxy climate information (e.g., tree-rings, historical evidences, cf. Brázdil et al. 2005 for an overview). Xoplaki et al. (2005) reconstructed and assessed spring and autumn temperatures back to 1500. By correlating the independent temperature reconstruction presented here with these reconstructions an overall excellent agreement is found for each season ($r_{season}$ > 0.95) and the uncertainties are comparable.

### 3.2 Seasonal European precipitation variations 1766–2000

Although in Europe different precipitation regimes can be identified, we focus on averages over the whole European region 1766 onward, in order to compare results with earlier studies (e.g., Pauling et al. 2006).

European winter precipitation anomalies from 1766 to 1844 (Fig. 3a) are slightly lower than during the twentieth century and further decrease to very low values from 1845 to 1905. After 1880 a positive trend of winter precipitation is found with maximum values from 1961 to 1972. The most recent winters again show a decrease in precipitation. Variability is high ($\sigma$ = 11 mm/season), so is the uncertainty of the reconstruction. The ±2 standard errors are about 21 mm/season in 1766 and steadily decrease to values of 11 mm/season around 1900.

Spring precipitation anomalies (Fig. 3b) are low for the 1766–1871 period. They reach a first positive peak 1880–1917 and a minimum 1933–1955. Spring precipitation then recovers to strongly positive anomalies 1963–1982 and decreases again in recent years. Precipitation variability is lower than winter with $\sigma$ = 7 mm/season. Uncertainties range from 10 to 7 mm/season.

Figure 3c presents the summer precipitation anomalies 1766–2000. Values are comparable with the twentieth century conditions between 1766 and 1852. From 1853 to 1874 a decrease in summer precipitation is found. After 1875 precipitation remains constant. Summer variability of precipitation is lowest compared with the other seasons ($\sigma$ = 7 mm/season). Uncertainties start with values of 7 mm/season and decrease to 4 mm/season for precipitation reconstructions prior to 1900.

Autumn precipitation anomalies 1766–2000 (Fig. 3d) show a clear cyclic variability on a timescale of 40–60 years. However, a comparison with the Atlantic Multidecadal Oscillation (AMO; e.g., Sutton and Hodson 2005) with a similar periodicity using cross wavelet analysis revealed no significant results (not shown). Recent values oscillate around the twentieth century mean with a strong increase since the 1990s. Variability is comparable with winter ($\sigma$ = 10 mm/season). Uncertainties are 15 mm/season after 1766 and improve to values of 10 mm/season at the end of the reconstruction period.

Due to the choice of a larger reconstruction area and the use of only station data, there are slight differences between the precipitation reconstruction presented in this study and the multi-proxy based reconstruction of Pauling et al. (2006). However, correlations between the seasonal reconstructions are overall high ($r_{season}$ > 0.8).

### 3.3 Covariability of temperature and precipitation 1766–2000

Covariability between LST and LSP are globally assessed for the CRU reanalyses (Mitchell and Jones 2005) back to 1901 by Déry and Wood (2005) and for the ERA-40 reanalyses (Simmons and Gibson 2000) over the 1979–2002

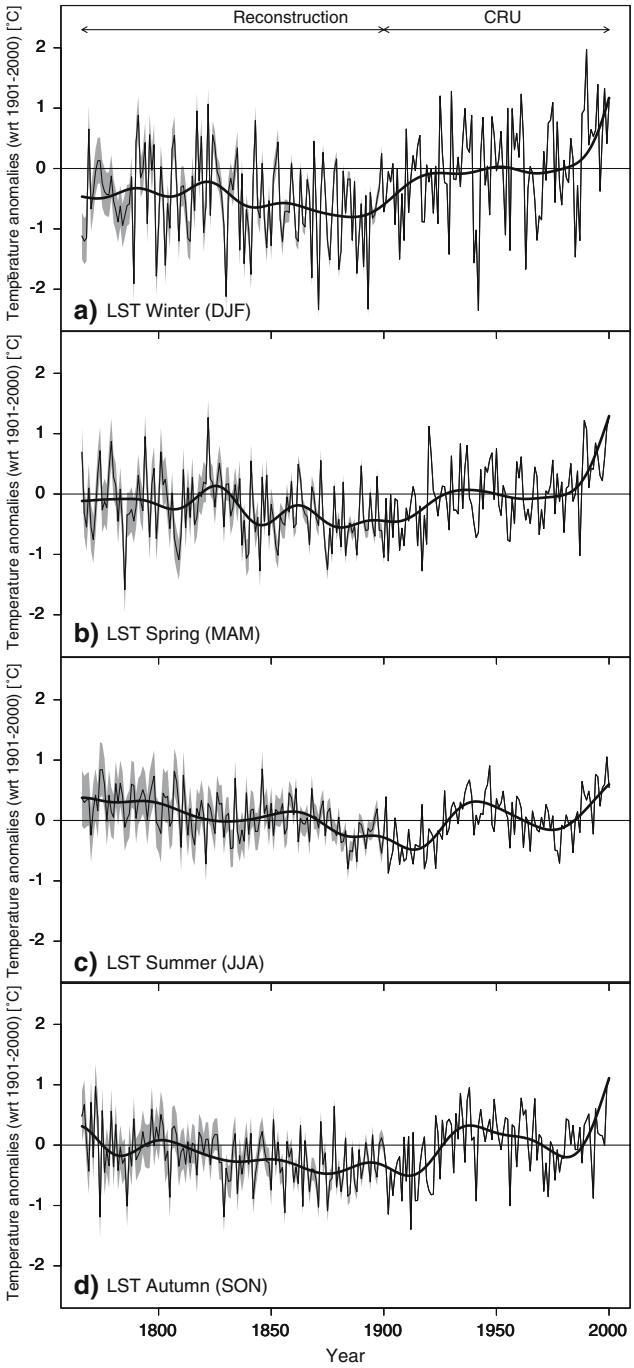


**Fig. 2** **a** Winter (DJF) mean European temperature anomalies 1766–2000 ([°C], reference period 1901–2000, *black line*). It is the average of the 18,000 grid points (7,652 over land). The *dark-grey* shading is the uncertainties of the reconstructions expressed as ±2 standard errors of the reconstruction. Note that the values from 1901 to 2000 is the CRU TS2 reanalysis (Mitchell and Jones 2005). The thick curve is a 31-year smoothing applied on the time series (Mann 2004). **b, c, d** Same as for **a** but for spring (**b**, MAM), summer (**c**, JJA), and autumn (**d,** SON)

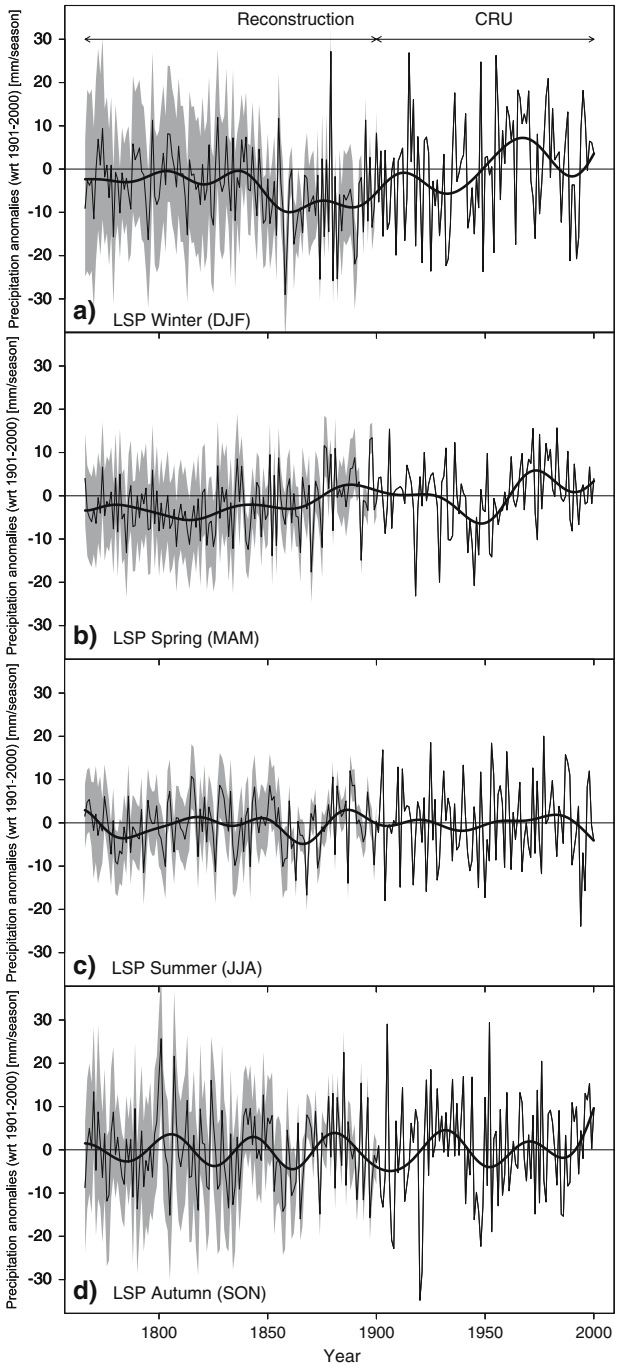


**Fig. 3** Same as Fig. 2 but for European precipitation anomalies 1766–2000 (mm/season)

period by Trenberth and Shea (2005). We extend these studies by assessing the covariability between the independent seasonal LST and LSP over Europe for the whole 1766–2000 period. Figure 4 exhibits the significant grid point to grid point correlations between detrended LSP and LST over the past 235 years for each climatological season. Confidence levels are calculated using a Monte Carlo approach to account for autocorrelation (Wilks 1995) leading to a robust 95% confidence level of 0.15 for a sample size of $n = 235$.

Winter correlations are positive along the coastal areas of northern Europe, the northern parts of France, and the east coast of Greenland and Iceland, and Spitsbergen. Negatively correlated regions cover the North-African coast and Sicily. This pattern points to advection related to a positive NAO. The coastal regions are influenced by warm ocean conditions, leading to an increased water holding capacity of extratropical cyclones compared with cold continental regions. Spring correlations (Fig. 4b) are comparable with the results for winter. The very north of the area is positively and southern Europe including North Africa is negatively correlated. However, the correlations are weaker than for winter. The extension of the negatively correlated area elongates much more to the north and covers the whole Mediterranean basin and parts of the British Isles. Again, this pattern reveals enhanced advective influence.

A completely different picture is represented by the summer correlations between LST and LSP (Fig. 4c). Significantly negative correlations dominate over the studied area including most parts of the European continent, the British Isles, western Greenland, and Spitsbergen. This is a hint that convective processes are important. Warm and dry conditions coincide (and vice versa). The autumn correlations (Fig. 4d) are similar to spring. However, compared with the spring pattern, the correlations around the Mediterranean basin are much weaker. Again, this pattern is more connected with advective processes.

### 3.4 Seasonal European climate pattern variability 1766–2000

In order to investigate the most important climate patterns that govern climate over Europe 1766–2000, we henceforth also consider the atmospheric circulation in the form of the independently reconstructed Z500 fields. As introduced in Sect. 2, combined EOFs are estimated using all three-climate variables. The focus is on the first three dominant EOFs that explain about 50% of the combined pressure, temperature and precipitation variability over Europe since 1766. Figure 5 presents the results of the leading combined linear EOF1 1766–2000 for each season and the corresponding PC time series. Results for EOF2 and EOF3 are presented in the electronic supplementary material (Figs. A, B, respectively).

EOF1 of winter (Fig. 5a–c; explaining 25.2% of the total combined climate variability), spring (Fig. 5e–g; 18.2%), and autumn (Fig. 5i–k; 17.7%) are very similar. The Z500 correlation pattern for winter (Fig. 5a) shows a dipole with one centre of action over Greenland/Iceland and the Iberian Peninsula. The corresponding temperature winter pattern (Fig. 5b) reveals positive correlations in northern and central Europe and negative ones over Greenland/Iceland and northern Africa. A warming in northern/central Europe is accompanied with a cooling over Greenland/Iceland and northern Africa (and vice versa, depending on the sign of the PCs in Fig. 5d). The precipitation pattern (Fig. 5c) shows positive correlations over northern Europe, the east coast of Greenland, Iceland, and Spitsbergen, but also over the southernmost eastern Mediterranean basin. The remaining part of the Mediterranean and Greenland is negatively correlated. Wet conditions over northern Europe are concurrent with drier conditions over the Mediterranean and vice versa. The normalised winter PC1 time series (Fig. 5d) fluctuates around the mean from 1766 to 1960. A trend to positive PC1 values is visible between 1961 and 1990. Recently, a drop in the PC time series is observed. During the strong positive trend 1961–1990, the Z500 had positive and negative anomalies over Spain and over Greenland/Iceland, respectively. This led to stronger than normal westerlies. Warm and wet air masses from the North Atlantic flow towards central and northern Europe resulting in positive LST and LSP anomalies. Spring and autumn show only small differences except for the explained variances and slight shifts of the southern centre of action. Particularly for autumn there is a north-eastern shift in Z500 and the corresponding LST and LSP fields. The temporal behaviour of spring PC1 (Fig. 5h) reveals also a trend to positive values since the 1960s and a recent decline similar to winter. This is not obvious for autumn PC1 (Fig. 5p).

The summer EOF1, however, reveals blocking-like patterns, in contrast to the three other seasons, which show NAO-type patterns. EOF2 + 3 (see electronic supplementary material, Figs. A + B) for winter, spring, and autumn exhibit blocking-like patterns. EOF3 of spring and autumn are rotated compared with winter EOF3. Summer EOF2 + 3 are NAO-like patterns and PC2 shows a positive trend being connected with warm and drier summer in central Europe during recent years. Note that the EOF analysis on seasonally averaged data results in the same patterns with a similar temporal and as expected higher explained variances. The EOF patterns are robust when comparing 100 years of data prior and after 1900 (not shown).

### 3.5 Combined annual EOFs and their relation to external forcing

In the following we focus on the temporal behaviour of the combined EOFs and address the question whether the combined EOFs are related to annually resolved radiative forcings ($CO_2$ from Etheridge et al. 1996; solar from Lean et al. 1995 and Crowley 2000; volcanic forcing from Crowley 2000). Note that the structure of annual combined EOFs is dominated by the winter season (cf. Fig. 5). As

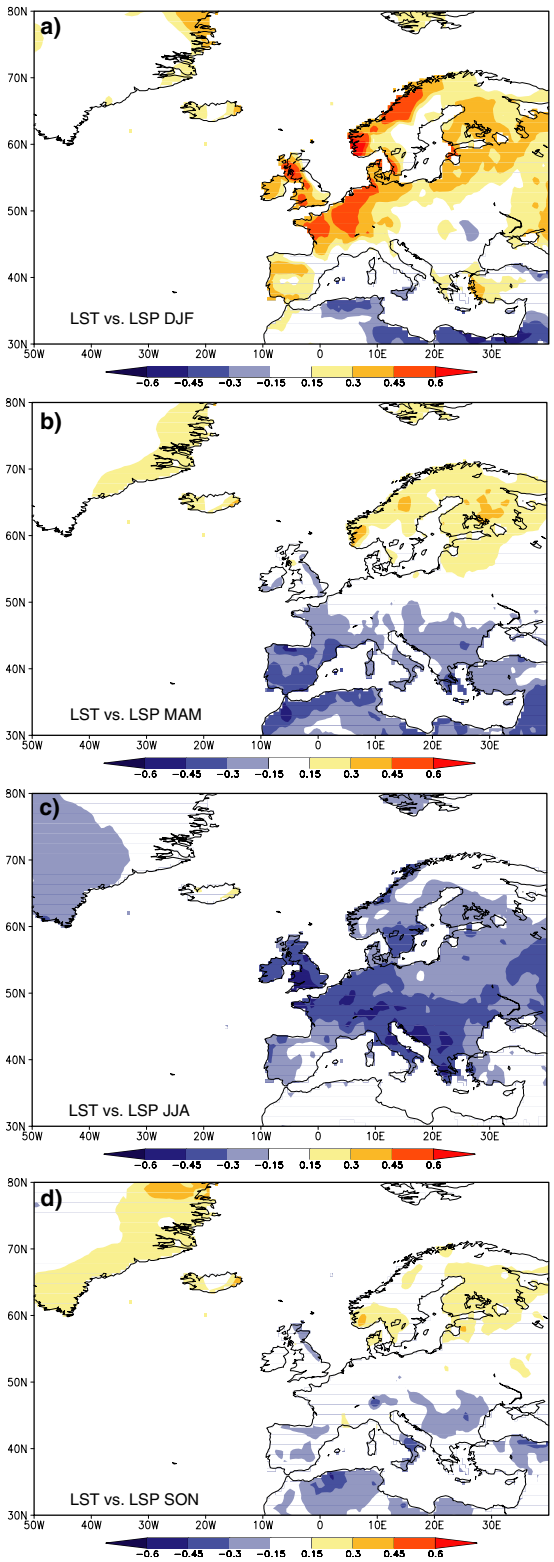


**Fig. 4** **a** Grid point to grid point correlation between detrended winter (DJF) mean anomalies of surface air temperature and precipitation amounts 1766–2000. The colours reveal regions that are significantly correlated on a 95% level using a robust Monte Carlo approach that considers autocorrelation. **b, c, d** The same as for **a** but for spring (**b**, MAM), summer (**c**, JJA), and autumn (**d**, SON), respectively

introduced in Sect. 2 we use wavelet, cross wavelet, and squared coherence wavelet techniques.

The wavelet spectrum of the leading combined EOF (explaining 19.4% of the total variance) shows a broad band from interannual to decadal variability in its PC1 with enhanced power about 4 years, between 8 and 16 years and a strong upward trend in the twentieth century (Fig. 6a). This indicates strong temperature, precipitation and pressure trends in the second half of the twentieth century (Hurrell and van Loon 1997; Raible et al. 2001; Wanner et al. 2001; Luterbacher et al. 2004; Casty et al. 2005a; Mitchell and Jones 2005; Raible et al. 2005; Xoplaki et al. 2003, 2004, 2005). Comparing PC1 with PC2 and PC3 (both not shown), we find a similar behaviour with exceptions that PC2 shows less pronounced decadal variability and that PC3 has no trend in the twentieth century. All wavelets tend to reduced variability over the entire spectral band in the late eighteenth and at the beginning of the nineteenth century. This could be traced back to the influence of the reduced performance of the LSP reconstruction for that period. The wavelet spectrum of $CO_2$ forcing (Fig. 6b) exhibits a significant peak with a similar power as PC1 for the same period in the twentieth century. The solar irradiance (Fig. 6c) shows the well-known 11-year cycle. In the wavelet spectrum of the volcanic forcing (Fig. 6d) significant peaks are found during the so-called Dalton Minimum, a phase of lowered solar but increased volcanic forcing from 1790 to 1830 (e.g., Wagner and Zorita 2005; Stendel et al. 2005; van der Schrier and Barkmeijer 2005). The series of eruptions in the 1980s and 1990s leads also to a wavelet spectral peak at about 8 years.

To focus on the linear connection of these time series, the squared wavelet coherence gives some information about the character of the correlation between the leading combined EOF and the forcings. Note that only significant areas are discussed that have a significantly increased power in corresponding cross wavelet spectrum (not shown). The wavelet coherence of the leading pattern and the $CO_2$ forcing (Fig. 7a) shows a clear relationship in the twentieth century where in both time series a strong trend is obvious. This trend is in phase as indicated by arrows pointing to the right.

The connection between the leading combined EOF and the solar forcing (Fig. 7b) shows a weak peak (in phase) from the 1940 to 1990, illustrating the contribution of increased solar activity in the twentieth century to the temperature trend. This resembles findings of modelling studies (e.g., Cubasch et al. 1997). All other significant structures in the coherence are not interpretable. For example, the phase shift is not stable in particular for the spectral band around periods of 11 years. The phase shift is 90 degrees from the 1960s onward, i.e., the PC1 leads the

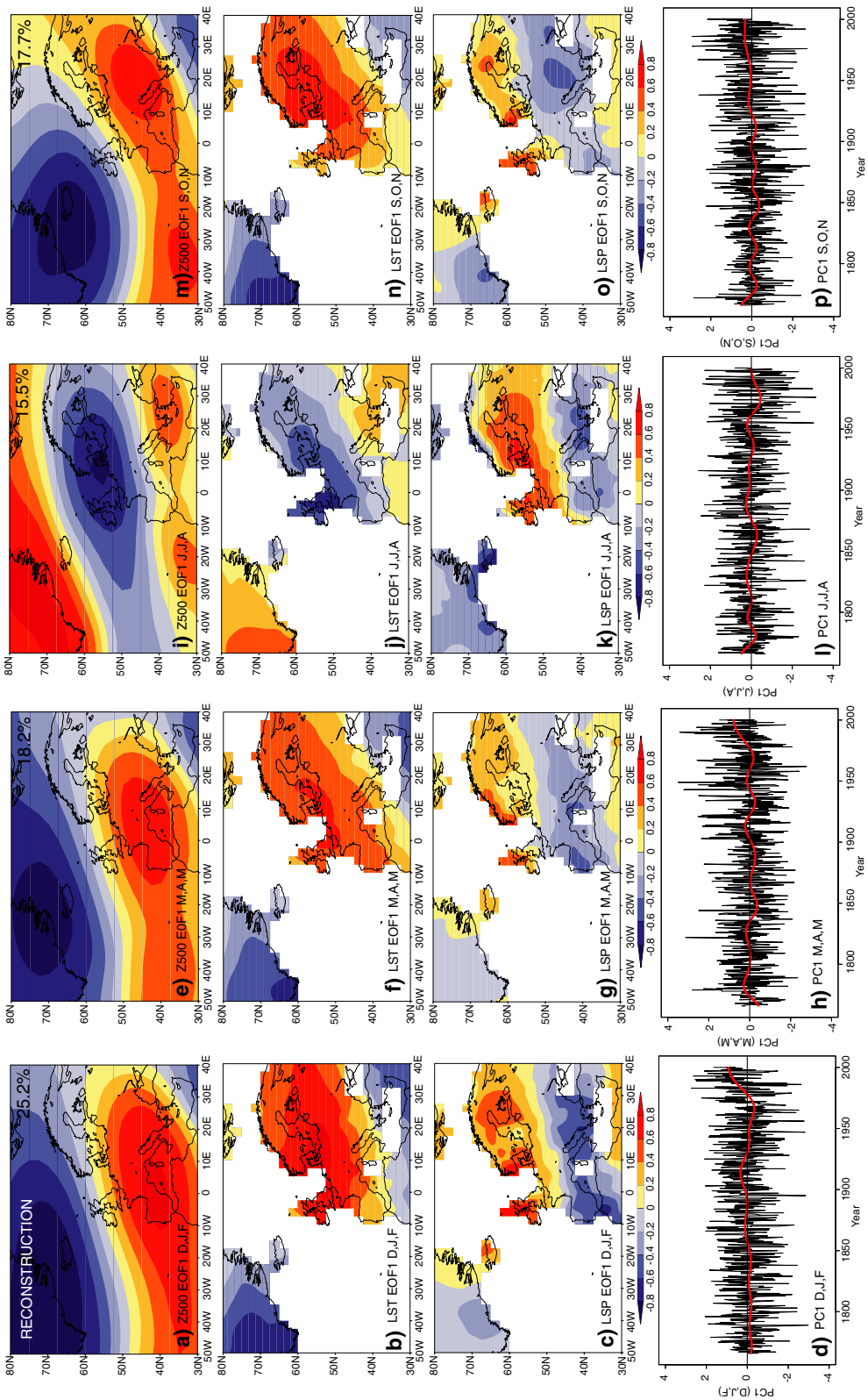


**Fig. 5** **a–c** Leading empirical orthogonal function (*EOF1*) winter (DJF) pattern of the *reconstructed* 500 hPa geopotential height (*Z500*, **a**), the land surface temperatures (*LST*, **b**), and land surface precipitation (*LSP*, **c**) obtained from the described combined linear EOF analysis 1766–2000. Values are correlations. **d** The corresponding normalised Principal Components (*PC*) 1766–2000 of the combined EOF1. Indicated by the red curve is the 31-year smoothing (Mann 2004). **e–p** The same as for **a–d** but for spring (**e–h**, MAM), summer (**i–l**, JJA), and autumn (**m–p,** SON) respectively. In the top right corners of figures **a, e, i** and **m** the explained variance of the respective EOF is shown

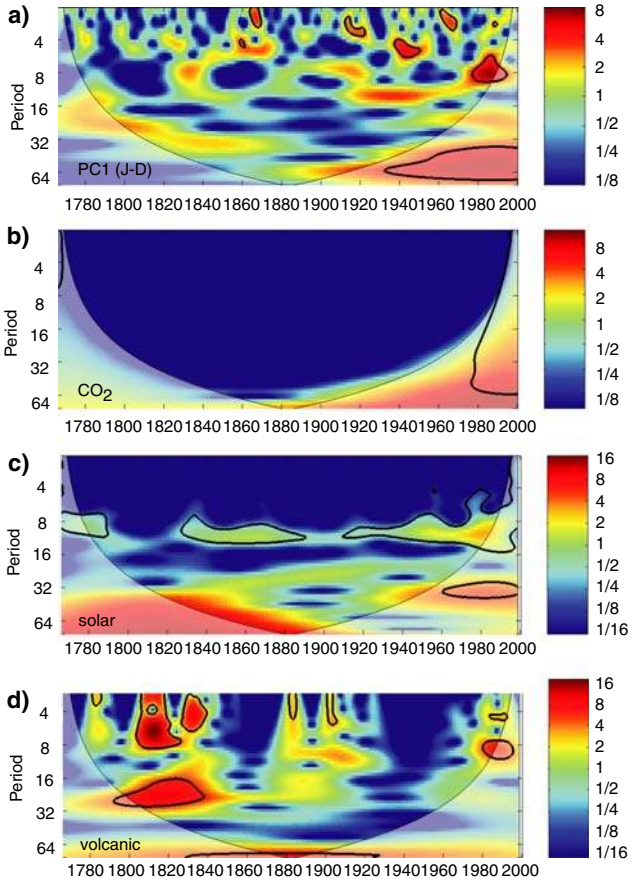


**Fig. 6** **a–d** The wavelet power spectrum of **a** the leading combined annual Principal Component (*PC1*) over Europe 1766–2000, **b** the $CO_2$ forcing (Etheridge et al. 1996), **c** the solar forcing (Lean et al. 1995; Crowley 2000), and **d** the volcanic forcing (Crowley 2000). The *thick black contour* is the 5% significance level against red noise. The cone influence where edge effects might be relevant is indicated as *lighter shadings*. *Colours* show the power (or variance). More details of the method are found in Torrence and Compo (1998)

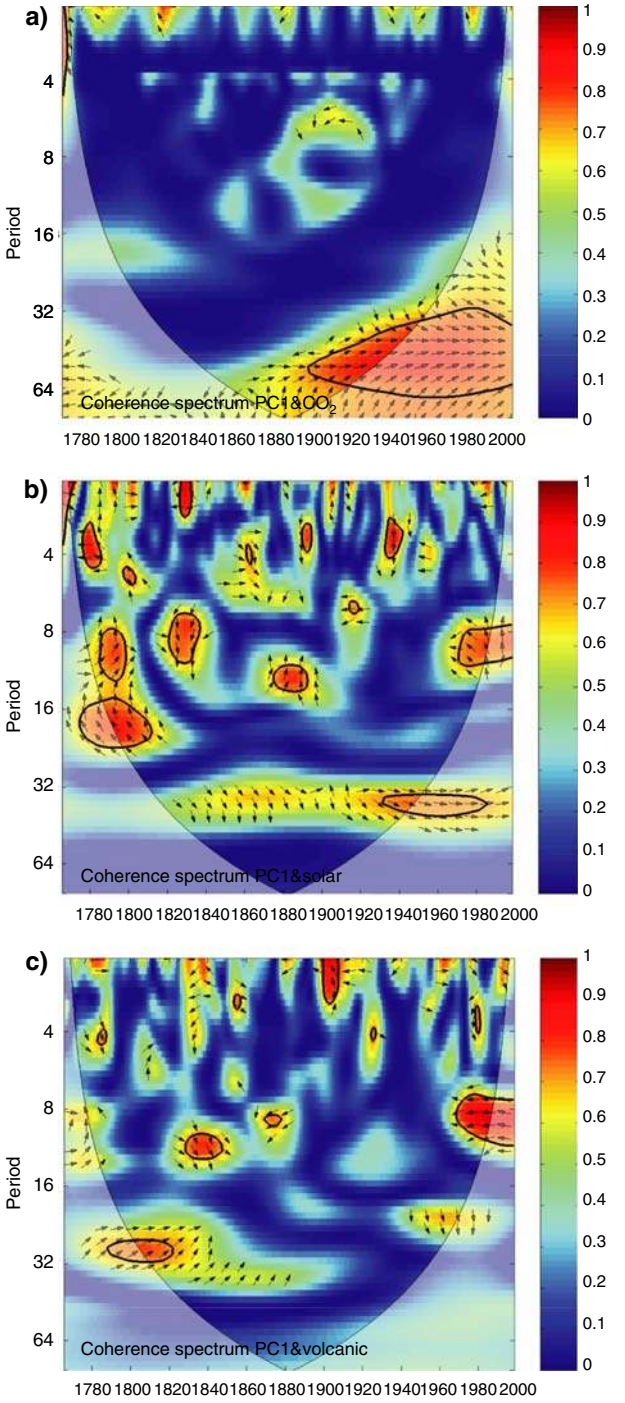


**Fig. 7** **a–c** The squared wavelet coherence between the PC1 and **a** the $CO_2$ forcing (Etheridge et al. 1996), **b** the solar forcing (Lean et al. 1995; Crowley 2000), and **c** the volcanic forcing (Crowley 2000). The *thick black contour* is the 5% significance level against red noise. The cone influence where edge effects might be relevant is indicated as lighter shadings. The coloured shading varies from zero to one, where one means perfect correlation in the time-frequency space. Arrows indicate the phase shift (the convention is: pointing right = in-phase; pointing left = anti-phase; pointing straight up = the PC1 leads the forcing by 90 degrees). More details about the method are found in Grinsted et al. (2004)

solar forcing by 90 degrees, but is 270 degrees from 1820 to 1840, i.e., the solar forcing leads the PC1 by 90 degrees.

For the volcanic forcing no connection to the leading combined EOF is found (Fig. 7c). Only the peak in the Dalton Minimum for the spectral band from 20 to 30 years shows an ''in-phase'' behaviour. This resembles findings of Yoshimori et al. (2005) where increased volcanic forcing leads to a positive phase of the NAO over the North Atlantic/European region. However, this is hardly interpretable. Again, for the second and third combined pattern we find no interpretable peaks with external forcings, therefore not shown.

Applying the methods to seasonal data we find that the annual wavelet, cross-wavelet spectra, and squared wavelet coherence are dominated by the winter (not shown). In summer, there is no trend in PC1 in the twentieth century and thus, there is no squared wavelet coherence with the

$CO_2$ forcing as in winter. With all other forcings and PCs we find no significant and interpretable wavelet coherence, suggesting that influences of the external forcing on the summer combined EOFs over the North Atlantic/European region are negligible.

To summarise we found that the natural (solar and volcanic) forcing has no direct and obvious connection to the combined annually Z500, LST, and LSP climate patterns for Europe, also not during winter and summer. Only the $CO_2$ forcing seems to be connected by its trend in the twentieth century. As this is observed in the region of the cone influence of the wavelet method, this result has to be treated with caution and still could also happen by chance as suggested by Wunsch (1999), Schneider et al. (2003), and Raible et al. (2005). Note also that it is not possible to detect non-linear responses with the methods, which is beyond the scope of this study.

## 4 Discussion and conclusion

Independent CFRs for Z500, LST, and LSP are a new tool besides past climate model runs to assess the dynamic of the climate prior to the reanalysis period and to put recent climate change into a longer term context. Luterbacher et al. (2002) presented SLP and Z500 reconstructions for Europe back to 1500. Recently, Luterbacher et al. (2004) computed high-resolution temperature CFR for Europe, so did Pauling et al. (2006) for precipitation. All used a multiproxy-approach including different types of data to reconstruct one distinct climate variable. However, when analysing these reconstructions regarding combined climate dynamics they suffer from dependence. In these studies SLP, Z500, and LST are estimated from a similar population, so no dynamical processes between these parameters can be independently observed and one runs into circular statements when comparing the different fields. The independent CFRs presented in this study rely fully on instrumental data. This reduces their length due to a limited number of pressure station data prior to 1766 that feed the statistical transfer functions. Although a smaller number of predictor station data than in Luterbacher et al. (2004), Xoplaki et al. (2005), and Pauling et al. (2006) was used, the uncertainties are comparable and small in particular for the Z500 and LST reconstruction. The independent CFRs are not multiproxy based and one does not mix station data of different frequency domains (e.g., temperature indices based on documentary evidence with low-frequency variability vs. station data) during the reconstruction process. In future, new methods to perform robust CFRs have to be developed after several deficiencies are known for regression based approaches (e.g., Bürger and Cubasch 2005; Telford and Birks 2005; Thejll and Schmith 2005).

Covariability between LST and LSP over Europe was seasonally assessed for the last 235 years. Trenberth and Shea (2005) presented a global ''covariability climatology'' for the last 23 years using ERA-40 reanalyses for temperature (Simmons and Gibson 2000) and the global precipitation climatology project (Adler et al. 2003). For winter (November–March) they observed positive correlation at high latitudes as an indication that warm moist advection from the extratropical cyclones lead to positive precipitation and temperature anomalies, and in contrast, that cold conditions limit the water holding capacity of the atmosphere. This is confirmed by our covariability analysis over the last 235 years, not only for winter, but also for spring and autumn (cf. Fig. 4a, b, d). During extended summers (March–September) Trenberth and Shea (2005) found mostly negative correlations over land, as dry conditions favour sunshine and reduced evaporative cooling. In contrast, wet summers are mainly cool, again confirmed by our results. Negative correlations dominate the European summer covariability since 1766 (cf. Fig. 4c). This is a clear hint, that convective processes play the most important role during summer. This is also supported from a recent study of Déry and Wood (2005), which analysed the CRU reanalyses (Mitchell and Jones 2005).

Fraedrich et al. (1993) combined 40 SLP, LST, and LSP stations and performed EOF analysis to describe winter climate patterns over Europe 1887–1986. Their winter EOF1 resembles a similar blocking-like pattern we found for winter as EOF2. EOF2 in Fraedrich et al. (1993) is very similar to the NAO pattern (EOF1) in this study. However, they differ in the percentage of the explained variances of EOF2 (16.8% here vs. 22.7%). This difference can be traced back to the choice of a different area, different data, and period. Casty et al. (2005a) used the same data to detect winter climate regimes in the combined fields of the Z500, LST, and LSP fields using nonlinear principal component analysis (Monahan 2000). They detected three winter climate regimes. The first two regimes are very similar to winter EOF1 and EOF2 described here. In the third regime the centre of action is shifted eastward and located over the British Isles compared to winter EOF3. Besides the methodological critics recently raised by Christiansen (2005), the detection of climate regimes in Casty et al. (2005a) led to dynamically meaningful patterns, comparable to those described in this study.

The combined EOFs are further compared with a simulation for the 1500–1990 period using the Community Climate System Model (CCSM version 3, Yeager et al. 2006), forced with solar irradiance, volcanic aerosols, and greenhouse gases. The T31 data were interpolated onto the 2.5° grid of the reconstructions and the combined EOF analysis is performed for the 1766–1990 period. The combined EOF1 of modelled Z500, LST, and LSP 1766–

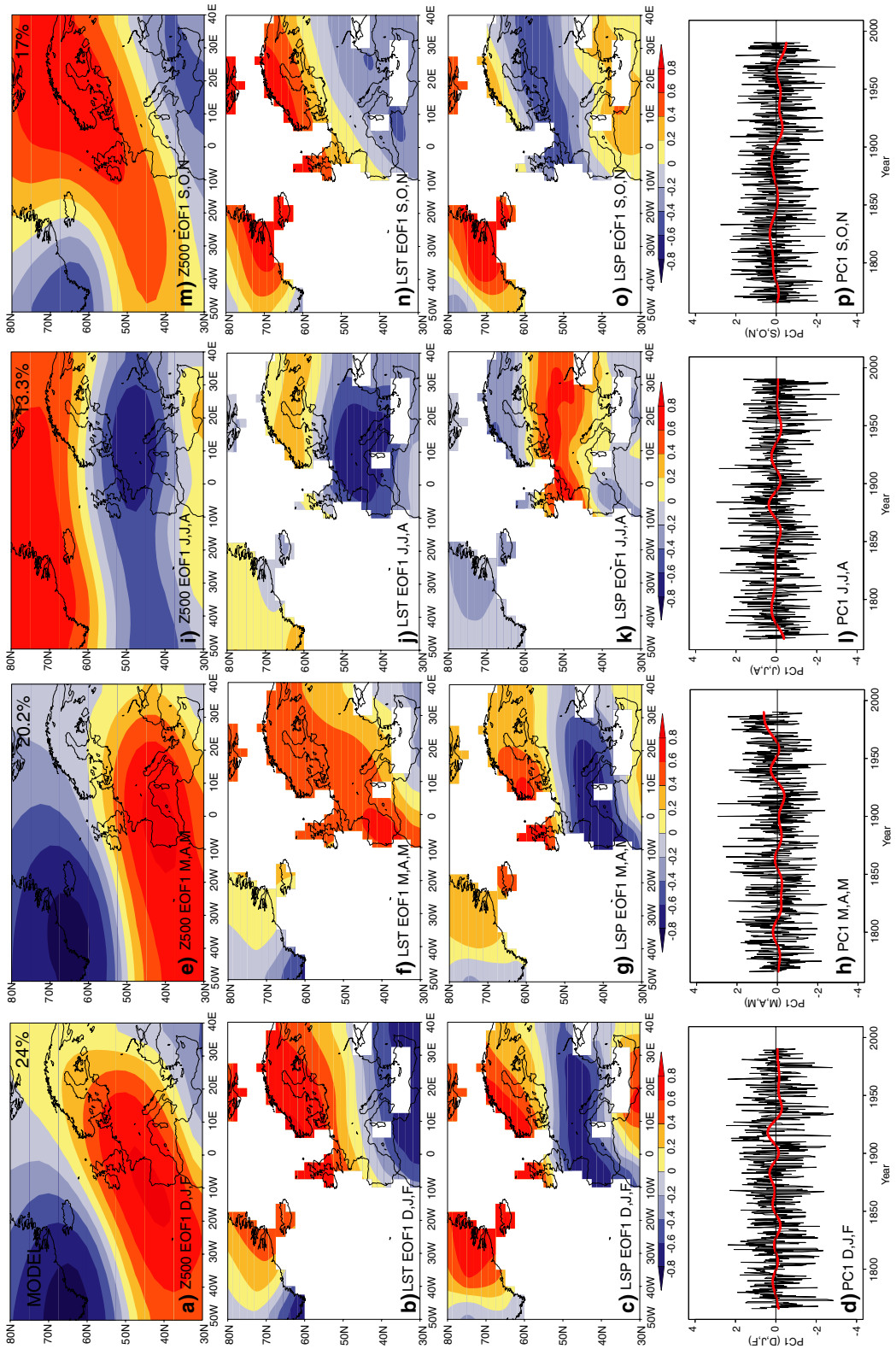


**Fig. 8** **a–c** Leading empirical orthogonal function (*EOF1*) winter (DJF) pattern of the *modelled* 500 hPa geopotential height (*Z500*, **a**), the land surface temperatures (*LST*, **b**), and land surface precipitation (*LSP*, **c**) obtained from the described combined linear EOF analysis 1766–1990. Values are correlations. **d** The corresponding normalised Principal Components (*PC*) 1766–1990 of the combined EOF1. Indicated by the red curve is the 31-year smoothing (Mann 2004). **e–p** The same as for **a–d** but for spring (**e–h**, MAM), summer (**i–l**, JJA), and autumn (**m–p**, SON), respectively. In the *top right corners* of figures **a, e, i** and **m** the explained variance of the respective EOF is shown

1990 (Fig. 8) revealed strong similarities with the spatial patterns for all seasons of the reconstruction (Fig. 5). Temporally, the PC1s behave differently in the reconstructed versus modelled climate, e.g., the observed positive trend of PC1 in recent years is absent in the modelled PC1. This could either be a hint that the observed trend is due to internal atmosphere–ocean variability or the fact that only one simulation is used in the analysis. This single model run is a random realisation of the past climate and for a complete comparison the focus should be on multi-model-ensembles, which is beyond the scope of this paper. The modelled combined EOF2 and 3 can be found in the electronic supplementary material (Figs. C and D, respectively).

A key issue in climate change studies is the detection of natural and anthropogenic signals in the climate system. The question to which part mankind is responsible for the upward trend in European temperatures in recent years (e.g., Jones and Mann 2004; Luterbacher et al. 2004; Xoplaki et al. 2005) or if it is a manifestation of natural internal variability in the form of climate patterns is of major interest. Long-term independent and high-resolution CFRs as presented in this study could help to answer these questions. It is now possible to study gridded and independent climate data for the last 235 year at least for Europe, i.e., more than twice as long as the CRU reanalyses (Mitchell and Jones 2005) today.

Various studies deal with the detection of external forcing on climate observations (e.g., Forest et al. 2002; Hegerl et al. 2004) or the output of complex climate models (e.g., Gillett et al. 2002; Yoshimori et al. 2005) or models of intermediate complexity (e.g., Knutti et al. 2002). At this point the reader is referred to the complete review on this topic by the International Ad Hoc Detection and Attribution Group (2005). We could not detect a direct and obvious linear connection between natural forcing, in the form of volcanic and solar radiative forcing, and the combined annually resolved Z500, LST and LSP climate patterns for Europe. The $CO_2$ forcing seems to be connected by its trend in the twentieth century, but again this result has to be treated with caution as it is detected at the margin of the wavelets where edge effects become important. Note that this connection is not apparent in the model simulation. One possible reason for not finding a connection between natural forcings and the European climate patterns is a signal detection problem over Europe as reported by Yoshimori et al. (2005) modelling the cold phase during the Maunder Minimum (1640–1715).

Still there are several limitations of the method used. The EOF analysis does not account for changes of the centre of action as illustrated by Christoph et al. (2000) and Raible et al. (2006). Another point is that the wavelet coherence only gives the linear relations in the time frequency space, e.g., the positive NAO response 1–2 years after volcanic eruptions as described by Yoshimori et al. (2005) and Fischer et al. (2007) was not detected by the method. We remark that the trend in the dominant climate pattern over Europe has shifted to negative values for the years since 2000 but Europe still experiences higher than average temperatures. This phenomenon has to be surveyed in forthcoming studies.

**Acknowledgments** CC and TFS are funded by the European commission fifth framework programme, Contract EVRI-2002–000413, project PACLIVA. We acknowledge support by the Swiss National Science Foundation through its NCCR Climate (MONALISA & PALVAREX II). JL also acknowledges the European Environment and Sustainable Development programme, projects SO&P (EVK2-CT-2002-00160) and EMULATE (EVK2-CT-2002-00161). We kindly acknowledge Dr. Elena Xoplaki and Dr. Andreas Pauling for providing their data and thank the two anonymous reviewers for their comments, which helped to improve this article. The package for performing cross-wavelet and wavelet coherence analysis is available at: http://www.pol.ac.uk/home/research/waveletcoherence/.

## References

Adler RF et al (2003) The version 2 global precipitation climatology project (GPCP) monthly precipitation analysis (1979-present). J Hydrometeorol 4:1147–1167

Barnston AG, Lizevey RE (1987) Classification, seasonality, and persistence of low-frequency atmospheric circulation patterns. Mon Wea Rev 115:1086–1126

Bjerknes J (1962) Synoptic survey of the interaction of sea and atmosphere in the North Atlantic. Geophys Norvegica 24:115–145

Brázdil R, Pfister C, Wanner H, von Storch H, Luterbacher J (2005) Historical climatology in Europe—the state of the art. Clim Change 70:363–430

Bretherton CS, Smith C, Wallace JM (1992) An intercomparison of methods for finding coupled patterns in climate data. J Clim 5:541–560

Briffa KR, Briffa KR, Osborn TJ, Schweingruber FH, Jones PD, Shiyatov SG, Vaganov EA (2002) Tree-ring width and density data around the Northern Hemisphere: Part 1, local and regional climate signals. Holocene 12:737–758

Brönnimann S, Luterbacher J (2004) Reconstructing Northern Hemisphere upper-level fields during World War II. Clim Dyn 22:499–510

Bürger G, Cubasch U (2005) Are multiproxy climate reconstructions robust? Geophys Res Lett 32. doi:10.1029/2005GL024155

Casty C, Handorf D, Sempf M (2005a) Combined climate winter regimes over the North Atlantic/European sector 1766–2000. Geophys Res Lett 32. doi:10.1029/2005GL022431

Casty C, Wanner H, Luterbacher J, Esper J, Böhm R (2005b) Temperature and precipitation variability in the European Alps since 1500. Int J Climatol 25:1855–1880. doi:10.1002/joc.1216

Christiansen B (2005) The shortcomings of nonlinear principal component analysis in identifying circulation regimes. J Clim 18:4814–4823

Christoph M, Ulbrich U, Oberhuber JM, Roeckner E (2000) The role of ocean dynamics for low-frequency fluctuations of the NAO in a coupled ocean–atmosphere GCM. J Clim 13:2536–2549

Crowley TJ (2000) Causes of climate change over the last 1000 years. Science 289:270–277

Cubasch U, Voss R, Hegerl GC, Waszkewitz J, Crowley TJ (1997) Simulation of the influence of solar radiation variations on the global climate with an ocean–atmosphere general circulation model. Clim Dyn 13:757–767

Déry SJ, Wood EF (2005) Observed twentieth century land surface air temperature and precipitation covariability. Geophys Res Lett 32. doi:10.1029/2005GL024234

Dommenget D, Latif M (2002) A cautionary note on the interpretation of EOF. J Clim 15:216–225

Etheridge D, Steele MLP, Langenfelds RL, Francey RJ, Barnola JM, Morgan VI (1996) Natural and anthropogenic changes in atmospheric $CO_2$ over the last 1000 years from air in Antarctic ice and firn. J Geophys Res 101:4115–4128

Forest CE, Stone PH, Sokolov AP, Allen MR, Webster MD (2002) Quantifying uncertainties in climate system properties with the use of recent observations. Science 295:113–117

Fischer EM, Luterbacher J, Zorita E, Tett SFB, Casty C, Wanner H (2007) European climate response to tropical volcanic eruptions over the last half millennium. Geophys Res Lett 34. doi:10.1029/2006GL027992

Fraedrich K (1994) ENSO impact on Europe?—a review. Tellus 46A:541–552

Fraedrich K, Bantzer C, Burkhardt U (1993) Winter climate anomalies in Europe and their associated circulation at 500 hPa. Clim Dyn 8:161–175

Gillett NP, Hegerl GC, Allen MR, Stott PA, Schnur R (2002) Reconciling two approaches to the detection of Anthropogenic influence on climate. J Clim 15:326–329

Graf H-F, Perlwitz J, Kirchner I (1994) Northern hemisphere tropospheric mid-latitude circulation after violent volcanic eruptions. Contr Atmos Phys 67:3–13

Grinsted A, Jevrejeva S, Moore J (2004) Application of the cross wavelet transform and wavelet coherence to geophysical time series. Nonlinear Proc Geophys 11:561–566

Groetzner A, Latif M, Barnett TP (1998) A decadal climate cycle in the North Atlantic Ocean as simulated by the ECHO coupled GCM, J Clim 11:831–847

Hannachi A, Jolliffe IT, Stephenson DB, Trendafilov N (2006) In search of simple structures in climate: simplifying EOFs. Int J Climatol 26:7–28

Hegerl GC, Zwiers FW, Kharin VV, Stott PA (2004) Detectability of anthropogenic changes in temperature and precipitation extremes. J Clim 17:3683–3700

Hoerling MP, Hurrell JW, Xu T (2001) Tropical origins for recent North Atlantic climate change. Science 292:90–92

Hoerling MP, Hurrell JW, Xu T, Bates GT, Phillips AS (2004) Twentieth century North Atlantic climate change. Part II: Understanding the effect of Indian Ocean warming. Clim Dyn 23:391–405

Hurrell JW (1995) Decadal trends in the North Atlantic Oscillation: regional temperatures and precipitation. Science 269:676–679

Hurrell JW (2003) The North Atlantic Oscillation: climatic significance and environmental impact. Geophys Monogr Ser 134:279

Hurrell JW, van Loon H (1997) Decadal variations in climate associated with the North Atlantic Oscillation. Clim Change 36:301–326

Hurrell JW, Hoerling MP, Phillips AS, Xu T (2004) Twentieth century North Atlantic climate change. Part I: Assessing determinism. Clim Dyn 23:371–389

James IN, James PM (1989) Ultra-low-frequency variability in a simple atmospheric circulation model. Nature 342:53–55

Jevrejeva S, Moore JC, Grinsted A (2003) Influence of the Arctic Oscillation and El Ninõ-Southern Oscillation (ENSO) on ice conditions in the Baltic Sea: The wavelet approach. J Geophys Res 108. doi:10.1029/2003JD003417

Jones PD, Mann ME (2004) Climate over past millennia. Rev Geophys 42. doi:10.1029/2003RG000143

Kalnay E et al (1996) The NCEP/NCAR 40-year reanalysis project. B Am Meteorol Soc 77:437–471

Kistler R et al (2001) The NCEP-NCAR 50-year reanalysis: monthly means CD-ROM and documentation. B Am Meteorol Soc 82:247–267

Knutti R, Stocker TF, Joos F, Plattner G-K (2002) Constraints on radiative forcing and future climate change from observations and climate model ensembles. Nature 416:719–723

Latif M, Roeckner E, Botzet M, Esch M, Haak H, Hagemann S, Jungclaus J, Legutke S, Marsland S, Mikolajewicz U, Mitchell J (2004) Reconstructing, monitoring, and predicting multidecadal-scale changes in the North Atlantic thermohaline circulation with sea surface temperature. J Clim 17:1605–1614

Lean J, Beer J, Bradley RS (1995) Reconstruction of solar irradiance since 1610: implications for climate change. Geophys Res Lett 22:3195–3198

Lorenz EN (1956) Empirical orthogonal functions and statistical weather prediction. Statistical Forecast Project Report 1, Dept. Meteorol. MIT, Cambridge

Luterbacher J, Xoplaki E, Dietrich D, Rickli R, Jacobeit J, Beck C, Gyalistras D, Schmutz C, Wanner H (2002) Reconstruction of sea level pressure fields over the Eastern North Atlantic and Europe back to 1500. Clim Dyn 18:545–561

Luterbacher J, Dietrich D, Xoplaki E, Grosjean M, Wanner H (2004) European seasonal and annual temperature variability, trends and extremes since 1500. Science 303:1499–1503

Mann ME (2004) On smoothing potentially non-stationary climate time series. Geophys Res Lett 31. doi:10.1029/2004GL019569

Mann ME, Rutherford S, Wahl E, Ammann C (2005) Testing the fidelity of methods used in proxy-based reconstructions of past climate. J Clim 18:4097–4107

Mitchell TD, Jones PD (2005) An improved method of constructing a database of monthly climate observations and associated high-resolution grids. Int J Climatol 25:693–712

Monahan AH (2000) Nonlinear principal component analysis by neural networks: theory and application to the Lorenz system. J Clim 13:821–835

Namias J (1948) Evolution of monthly mean circulation and weather patterns. Trans Am Geophys Union 29:777–788

Pauling A, Luterbacher J, Casty C, Wanner H (2006) Five hundred years of gridded high-resolution precipitation reconstructions over Europe and the connection to large-scale circulation. Clim Dyn 26:387–405

Perlwitz J, Graf H-F (2001) Troposphere–stratosphere dynamic coupling under strong and weak polar vortex conditions. Geophys Res Lett 28:271–274

Raible CC, Luksch U, Fraedrich K, Voss R (2001) North Atlantic decadal regimes in a coupled GCM simulation. Clim Dyn 18:321–330

Raible CC, Stocker TF, Yoshimori M, Renold M, Beyerle U, Casty C, Luterbacher J (2005) Northern Hemispheric trends of pressure indices and atmospheric circulation patterns in observations, reconstructions, and coupled GCM simulations. J Clim 18:3968–3982

Raible CC, Casty C, Esper J, Luterbacher J, Pauling A, Rösch AC, Schär C, Tschuck P, Vidale P-L, Wild M, Wanner H (2006) Climate variability—observations, reconstructions, and model simulations for the Atlantic-European and Alpine region from 1500–2100. Clim Change. doi:10.1007/s10584–006-9061-2

Rowntree P (1972) The influence of tropical east Pacific Ocean temperature on the atmosphere. Quart J Roy Meteor Soc 98:290–321

Rutherford S, Mann ME, Delworth TL, Stouffer RJ (2003) Climate field reconstruction under stationary and nonstationary forcing. J Clim 16:462–479

Rutherford S, Mann ME, Osborn TJ, Bradley RS, Briffa KR, Hughes MK, Jones PD (2005) Proxy-based Northern Hemisphere surface temperature reconstructions: sensitivity to method, predictor network, target season, and target domain. J Clim 18:2308–2329

Schmutz C, Gyalistras D, Luterbacher J, Wanner H (2001) Reconstruction of monthly 700, 500 and 300 hPa geopotential height fields in the European and Eastern North Atlantic region for the period 1901–1947. Clim Res 18:81–193

Schneider EK, Bengtsson L, Hu Z-Z (2003) Forcing of Northern Hemisphere climate trends. J Atmos Sci 60:1504–1521

Shindell DT, Schmidt GA, Mann ME, Faluvegi G (2004) Dynamic winter climate response to large tropical volcanic eruptions since 1600. J Geophys Res 109. doi:10.1029/2003JD004151

Simmons AJ, Gibson JK (2000) The ERA-40 project plan. Technical Report, ECMWF, Reading, pp 63

Stephenson DB, Hannachi A, O'Neill A (2003) On the existence of multiple climate regimes. Quat J Roy Meteorol Soc 130:583–606

Stendel M, Mogensen IA, Christensen JH (2005) Influence of various forcings on global climate in historical times using a coupled atmosphere–ocean general circulation model. Clim Dyn 25. doi:10.1007/s00382-005-0041-4

Sutton RT, Hodson DLR (2005) Atlantic ocean forcing of North American and European summer climate. Science 309:115–118

Telford RJ, Birks HJB (2005) The secret assumption of transfer functions: problems with spatial autocorrelation in evaluating model performance. Quat Sci Rev 24:2173–2179

The International Ad Hoc Detection, Attribution Group (2005) Detecting and attributing external influences on the climate system: a review of recent advances. J Clim 18:1291–1314

Thejll P, Schmith T (2005) Limitations on regression analysis due to serially correlated residuals: application to climate reconstruction from proxies. J Geophys Res 110. doi:10.1029/2005JD005895

Torrence C, Compo GP (1998) A practical guide to wavelet analysis. B Am Meteorol Soc 79:61–78

Trenberth KE, Shea DJ (2005) Relationships between precipitation and surface temperature. Geophys Res Lett 32. doi:10.1029/2005GL022760

van der Schrier G, Barkmeijer J (2005) Bjerknes' hypothesis on the coldness during AD 1790–1820 revisited. Clim Dyn 24:355–371

Wagner S, Zorita E (2005) The influence of volcanic, solar and $CO_2$ forcing on the temperatures in the Dalton Minimum (1790–1830): a model study. Clim Dyn 25:205–218

Wanner H, Brönnimann S, Casty C, Gyalistras D, Luterbacher J, Schmutz C, Stephenson DB, Xoplaki E (2001) North Atlantic Oscillation—concepts and studies. Surv Geophys 22:321–381

Wilks DS (1995) Statistical methods in the atmospheric sciences: an introduction. Academic, London

Wunsch C (1999) The interpretation of short climate records, with comments on the North Atlantic and Southern Oscillation. Br Am Meteorol Soc 80:245–255

Xoplaki E, González-Rouco FJ, Luterbacher J, Wanner H (2003) Mediterranean summer air temperature variability and its connection to the large-scale atmospheric circulation and SSTs. Clim Dyn 20:723–739

Xoplaki E, Gonzalez-Rouco JF, Luterbacher J, Wanner H (2004) Wet season Mediterranean precipitation variability: influence of large-scale dynamics and trends. Clim Dyn 23:3–78

Xoplaki E, Luterbacher J, Paeth H, Dietrich D, Steiner N, Grosjean M, Wanner H (2005) European spring and autumn temperature variability and change of extremes over the last half millennium. Geophys Res Lett 32. doi:10.1029/2005GL023424

Yeager ST, Shields CA, Large WG, Hack JJ (2006) The low-resolution CCSM3. J Clim 19:2545–2566

Yoshimori M, Stocker TF, Raible CC, Renold M (2005) Externally-forced and internal variability in ensemble climate simulations of the Maunder Minimum. J Clim 18:4253–4270